EFDA–JET–R(13)01

E. de la Luna, J. Fessey, L. Barrera, P. Trimble
and M. Buckley

Frequency Range Extension of the ECE Radiometer on JET (EP2 project/2006-2008)

Frequency Range Extension of the ECE Radiometer on JET (EP2 project/2006-2008)

E. de la Luna[1,2], J. Fessey[3], L. Barrera[1], P. Trimble[3] and M. Buckley[3]

[1]*Laboratorio Nacional de Fusión, EURATOM-CIEMAT Association, 28040 Madrid, Spain*
[2]*EFDA-JET CSU, Culham Science Centre, Abingdon, OX14 3DB, UK*
[3]*EURATOM/UKAEA Fusion Association, Culham Science Centre, OX14 3DB, UK*

Frequency range extension of the ECE radiometer on JET (EP2 project/2006-2008)

E. de la Luna[1,2], J. Fessey[3], L. Barrera[1], P. Trimble[3], M. Buckley[3]

[1] Laboratorio Nacional de Fusión. EURATOM-CIEMAT Association, 28040 Madrid, Spain

[2]EFDA-JET CSU, Culham Science Centre, Abingdon, OX14 3DB, UK

[3]CCFE, Culham Science Centre, Abingdon OX14 3DB, UK

Abstract. An extensive upgrade of the JET radiometer was implemented in 2008 in order to further enhance the performance of the system. Six new high frequency mixers were added, bringing the total number of receivers to twelve. In this way the radiometer provides continuos frequency coverage from 69 GHz to 207 GHz, enabling the diagnostic to operate over a wider range of plasma conditions. This report describes the changes introduced in the system architecture in order to add the new hardware and gives some illustrative examples of the improved performance of the diagnostic.

1. Introduction

For many years now, the multichannel heterodyne radiometer, known as KK3, has been routinely used in JET to provide time resolved electron temperature profiles. The radiometer has been in operation since 1993 [1] and during its lifetime it has been modified at various times to improve its measurement performance. In 1995, the operating frequency bandwidth of the radiometer was extended to provide continuous coverage from 69−139 GHz and the bandwidth of the IF filters was reduced from 500 MHz to 250 MHz to improve the spatial resolution of the measurements [2]. The system comprised six independent heterodyne receivers and had a total of 48 channels. In 2002 a major upgrade took place [3], focused on increasing the number of channels from 48 to 96 and since then till 2008 the architecture of the system remained stable.

The JET radiometer was originally designed to allow the observation of different polarizations, for first harmonic O-mode (denoted by 1O-mode) or second harmonic X-mode (denoted by 2X-mode) electron cyclotron emission (ECE) measurements. The 2X-mode was used for the lower fields and larger radii and the 1O-mode for higher fields ($B_0 > 2.4$ T). This additional flexibility provided a wide radial coverage for most of the magnetic fields used at JET (1.7 T $< B_0 <$ 4 T) using a reduced number of mixers. However, this set-up was not fully optimized for high field operation in JET in which the 1O-mode radiation could suffer cutoff in high-density plasmas, being the cutoff density for 1O-mode ECE measurements half that of the 2X-mode.

In 2006 an extensive enhancement of the radiometer was approved and the upgraded system began its operation in June 2008. The main goal of project was to increase the range of accessible electron densities at which reliable ECE measurements can be performed in JET by extending the observation of 2X-mode emission at higher magnetic fields. This was accomplished by increasing the number of receivers available up to 12, with the corresponding increase in frequency coverage (up to 207 GHz), and adding the associated IF amplifiers and switching circuits. The number of channels did not change (96 channels), therefore no modifications of the downstream systems (video amplifiers and data acquisition) were required. This document describes the modifications carried out in the radiometer to increase its operating frequency range. The improved performance of the diagnostic is illustrated using some of the first results obtained during the commissioning of the upgraded instrument at JET.

2. Scientific background and motivation for the enhancement

Two requirements are essential for making reliable T_e measurements by ECE (see [4] for a recent review and references therein):

a) the optical depth of the plasma must be sufficiently high so that the emission is at black-body level (so that the emitted intensity is proportional to T_e)

b) the plasma electron density must be low enough that the emitting frequency is clearly above the cutoff frequencies (so that the radiation is able to leave the plasma and reach the detecting system). The cutoff occurs for the 1O-mode at the plasma frequency, $\omega_p = \sqrt{n_e e^2/(\epsilon_0 m_e)}$, and for the 2X-mode at the right hand cutoff frequency, $\omega_R = \frac{1}{2}[\omega_{ec} + (\omega_{ec}^2 + 4\omega_p^2)^{1/2}]$, where ω_{ec} is the electron cyclotron frequency. Note that refraction effects will become increasingly important when the emitting frequency is close to the cutoff frequency.

In general, for JET plasma conditions, the temperature and the density of the bulk plasma are high enough to ensure that the first condition is met for the 2X-mode and the 1O-mode ECE. Optical thickness quickly drops towards the plasma edge and in some cases it may be insufficient to provide reliable T_e measurements in this region. The second condition imposes a maximum electron density (that depends on the magnetic field and the polarization mode) below which ECE measurements are possible. These two restrictions are more severe for the 1O-mode since both, the optical depth and cutoff density, are lower than that of the 2X-mode. The cutoff density ($n_{e,cutoff}$) for each polarization can be written as:

$$\text{O-mode: } n_{e,cutoff}^{O-mode} = s^2(\epsilon_0 B_0^2)/m_e = 1.94 \times B_0^2 \times 10^{19} \text{ m}^{-3}$$

$$\text{X-mode: } n_{e,cutoff}^{X-mode} = s(s-1)(\epsilon_0 B_0^2)/m_e$$

where s is the harmonic number. As can be seen in figure 1, the usage of O-mode radiation imposes an additional limit in the range of electron densities at which ECE

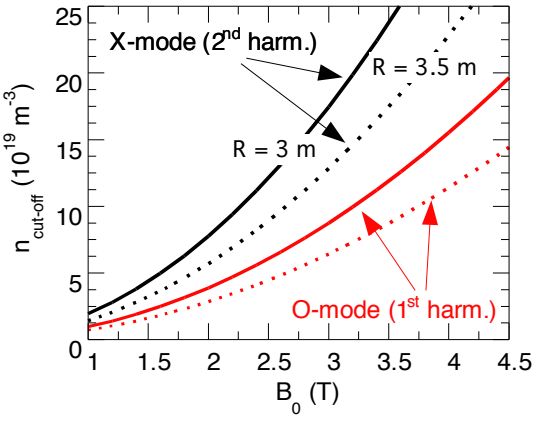

Figure 1. Cutoff electron density for the fundamental O-mode ($\omega = \omega_{ec}$) and the second harmonic X-mode ($\omega = 2\omega_{ec}$) in JET vs the central magnetic field for two radii: $R = 3$ m (continuous line) and $R = 3.5$ m (dotted line)

measurements can be obtained, being the cutoff density of the 2X-mode emission twice that of the 1O-mode.

This limitation is particularly relevant for high field operation at JET. At $B_0 > 2.5$ T, JET operates at relatively high densities ($n_e > 6 \times 10^{19}$ m^{-3}) and the radiation temperature measured by the existing radiometer (using 1O-mode) was often in cut-off during the H-mode phase. This effect is illustrated in figure 2, where the temporal evolution of the central electron temperature (T_e) measured by the radiometer (1O-mode) and the Michelson interferometer (2X-mode) for a typical JET discharge (#61314) with $B_0 = 2.7$ T is compared. In this pulse, 15 MW of neutral beam heating (NBI) are applied between 16-24 sec. As the density rises the emitting frequency becomes lower than the cutoff frequency ($\omega_{ec} < \omega_p$, for 1O-mode emission) and the radiation can no longer propagate out from its emitting location to the detection system. This causes an abrupt loss of the detected signal and the radiation temperature derived from ECE is no longer representative of the local T_e values. On the other hand, the 2X-mode emission measured by the Michelson interferometer (Δt =17 ms and $\Delta r = 20$ cm) still provides a reliable measurement of the electron temperature.

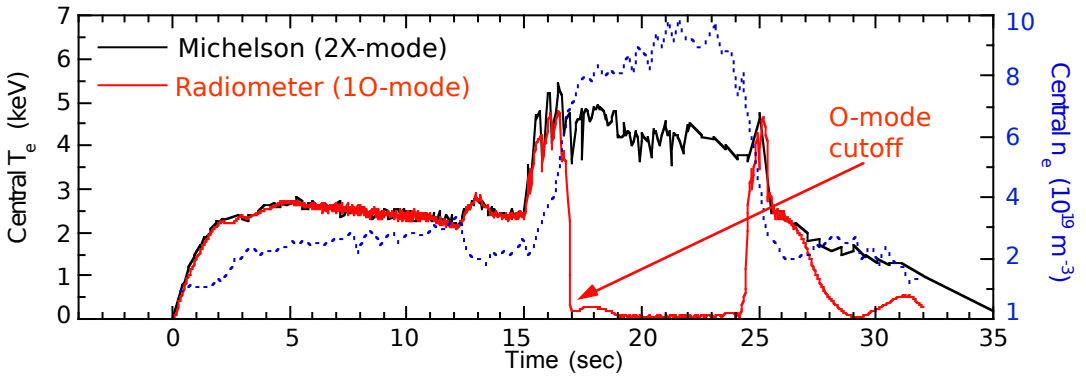

Figure 2. Central T_e measured by ECE diagnostics in a high-density discharge in JET (#61314: $P_{NBI} = 15$ MW, $B_0 = 2.7$ T) together with the central density measured by the Thomson Scattering system (dotted line). In high magnetic field operation (B_0 >2.5 T) at JET, the 1O-mode ECE is often in cutoff during the H-mode phase of the discharge.

The main purpose of this enhancement project was to increase the spectral coverage of the radiometer in order to extend the use of 2X-mode measurements for all magnetic fields (for $B_0 > 1.7$ T) used in JET (central T_e data in X-mode was limited to $B_0 < 2.5$ T with the existing system). Below 1.6 T the required resonant frequencies are outside the frequency bandwidth of the instrument. Since the intrinsic spatial resolution (natural line width of the EC radiation) for 2X-mode measurements (higher optical thickness) is better than that of 1O-mode measurements [5, 6], the upgrade will also have a positive impact on the spatial resolution of the T_e measurements at high magnetic field operation. We also took the opportunity to implement a better thermal control of the gain stability of the instrument with the aim of improving the long-term stability of the system.

3. Basic description of the JET radiometer

The JET heterodyne radiometer has been described in some detail elsewhere [2, 3] and only a summary is given here. The ECE radiation is collected from the low field side, perpendicular to the B-field along the major radius in the equatorial mid-plane and is transmitted by rectangular oversize waveguides over a distance of ∼50 m to the Diagnostic Hall, where the radiometer is located. The oversize waveguides carry both orthogonal linear polarizations (O-mode and X-mode) and a series of non-polarizing wire grid splitters is used to split the input radiation 6 ways. In each of these 6 branches a polarizing splitter separates the horizontal and vertical components of the emission. After the splitters, tapers reduce the waveguide to fundamental waveguide (depending on the receiver bandwidth) and only one of the two polarization modes is fed to the heterodyne receivers via a motorized waveguide switch. In that way, each receiver can be independently set-up for either 1O-mode or 2X-mode ECE measurements. The receive signal is split into 96 channels. After the waveguide switch used to select the polarization to be observed, each of the channels is set-up as follows:

- Heterodyne receiver, consisting of a band-pass filter to suppress unwanted bands (image), a fixed frequency local oscillator and a broadband balanced mixer. This is used to down-convert the detected radiation into an intermediate frequency (IF) signal (6-18 GHz).
- A couple of IF amplifiers (30-50 dB). Calibrated attenuators are used to control the linear response of the system.
- A set of IF switches to select which mixers are connected to the acquisition chain.
- Power dividers (2 ways, 3 ways and 4 ways splitters) to divide the input signal into the 96 channels.
- Band pass filter (central frequencies between 6 to18 GHz, 250 MHz bandwidth)
- Un-biased Schotkky detector (1MHz bandwidth)
- Video pre-amplifier (1MHz bandwidth, gain 100×)

- Main amplifier (2 amplification stage) with variable gain (2× to 100×) and variable low pass filter (1 kHz, 5 KHz) and a fast monitoring output (250 KHz) after the first amplification stage.

More details on the architecture of the receivers and the IF filter banks can be found in [3]. The radiometer is connected to three separate acquisition systems. There is one fast acquisition systems (250-500 kHz) that are used to study fast events such as ELM precursor or coherent MHD modes. The second is a slow (5 kHz) VME based digitiser (50k samples/channel) for profile temperature measurements and the third is the one with the slowest sampling rate (40 Hz) integrated within the Real Time Control system. The acquisition system used for profile measurements has been replaced by UXD7 modules (capable of operating at sampling rates of 200 kHz) in 2011.

The selection of the receiver and the polarization to be observed by each mixer, which is dependent on the magnetic field and the region of the plasma from which the data is requested, can be remotely controlled by a software program running in the JET Control Room. The settings of the video main amplifier (gain and bandwidth) as well as the input parameters for the data acquisition (number and times of acquisition windows and the sampling rates) are also set using this program.

4. Technical description of the radiometer upgrade

The project goals were accomplished by adding 6 new high frequency receivers to the instrument with the associated amplifiers and switching circuits without modifying the waveguide transmission line. Transmission line and the data acquisition section (including the filter-bank, the detectors and video amplifiers) remain unchanged and only the radiometer front-end was modified. Due to the importance of the KK3 radiometer for the JET physics program, the safest approach was chosen in the design of the upgrade, which was to built a complete new RF section without modifying the transmission line. This option makes a better use of the signal availability as well as allows keeping the existing RF section as a back-up solution in case of failure of any of the new receivers. In the following sections the differences between the previous and the upgraded system are described.

4.1. Status of the diagnostic (receiver section) before the 2008 upgrade

A block diagram of the original system is shown in figure 3. This is a brief summary of the status of the original system:

- The radiometer included 6 heterodyne receivers, which provided continuous frequency coverage from 69 to 139 GHz.
- The polarization of the radiation for each of the receivers was selected by means of a 2-ways motorized waveguide switch. The waveguide switches for receivers 1 and 2 were old units controlled through a driver installed in the KK3 cubicle, while for the receivers 3 to 6 the waveguide switches were controlled via GPIB.

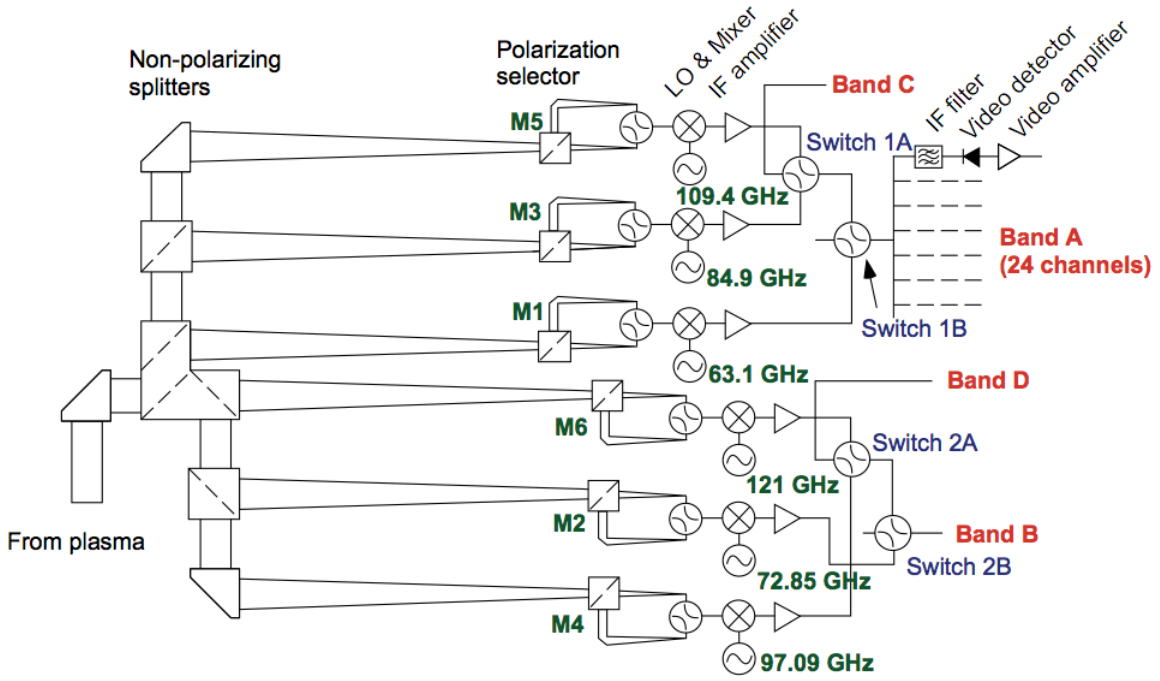

Figure 3. Schematic layout of the JET radiometer before the 2008 upgrade

- For each JET pulse data, 4 adjacent receivers were acquired, with 24 channels per receiver (total number of channels = 96). The selection of which receivers were connected to the acquisition chain was carried out by two sets of IF switches (see figure 3).
- Power dividers (2-ways, 3-ways and 4-ways splitters) were used to divide the input signal into the 96 channels
- The 96 channels were divided into four acquisition bands, with a 24 channels per band, named A (channels 1-24), B (channels 25-48), C (channels 49-72) and D (channels 73-96). Each of the bands had a 12 GHz bandwidth (6-18 GHz) with a distance between channels that goes from 0.5 GHz at the beginning of the band to 1 GHz at the end of the band.

4.2. Main changes in the diagnostics

The block diagram of the final radiometer setup after the upgrade is shown in figure 4. The main changes in the diagnostic with respect to the previous system are:

- The number of receivers has increased from 6 to 12, providing continuous frequency coverage from 69 to 207 GHz. The frequency of the local oscillator (LO) for all receivers, including the new ones (7-12), as well as their frequency coverage is shown in the Table 1. In the rest of the text the receivers will appear as M1 to M12.
- The architecture of the new receivers is similar to that of the existing ones [3].

Receiver	LO frequency (GHz)	RF frequency range (GHz)
M1	63.1 GHz	69−81 GHz
M2	72.8 GHz	79−91 GHz
M3	84.9 GHz	91−103 GHz
M4	97.1 GHz	103−115 GHz
M5	109.4 GHz	115−127 GHz
M6	121 GHz	127−139 GHz
M7	133.6 GHz	139.6−151.6 GHz
M8	144.7 GHz	150.7−162.7 GHz
M9	155.8 GHz	161.8−173.8 GHz
M10	166.8 GHz	172.8−184.8 GHz
M11	177.7 GHz	183.7−195.7 GHz
M12	188.6 GHz	194.6−206.6 GHz

Table 1. Local oscillator frequency and frequency bandwidth (IF bandwidth=6-18 GHz) for each of the mixers. M7 to M12 are the new high frequency mixers installed in 2008

- The entire IF amplifier section (for old and new receivers) was replaced by temperature controlled amplifiers with better characteristics in terms of noise and gain stability.
- New waveguide motorized switches were also installed. Two different type of RF waveguide switches are used: (a) 2-ways switches for receivers 4, 5 and 6 (no changes for those receivers) and (b) 3-ways switches for receivers 1, 2 and 3.
  The 3-ways switches allow not only the selection of the polarization to be observed but also the inclusion of the new 6 receivers (7 to 12) without modifying the oversized waveguide path (see figure 4). With this set-up it is possible to select either one of the low-frequency mixers (1, 2, 3) or two of the new high-frequency (7-8, 9-10, 11-12). This approach is based on the fact that two high-frequency receivers operating in 2X-mode provide approximately the same radial coverage that one single low-frequency receiver in 1O-mode due to the different gradient of the second and first harmonic electron cyclotron frequency profile. A brief description of the operation of waveguide switches can be found in Section 4.2.1
- A new IF switches matrix (20 inputs / 8 outputs) has been installed in order to accommodate the new 6 receivers in the existing data acquisition structure, so that at any time a sub-set (4 to 6) of the 12 mixer available can be connected to the data acquisition chain. The operation of the IF switch matrix is summarized in Section 4.2.2
- The IF switches matrix as well as all the waveguide switches are now controlled via a GPIB interface.
- To include the high-frequency receivers the arrangement of the IF filters in each

of the acquisition bands had to be changed. With the previous system the 96 channels were distributed in 4 bands (6-18 GHz), with 24 channels per band (band A:1-24, B:25-48, C:49-72, D:73-96). For the new system, each of these bands has been divided into two sub-bands (A1, A2, B1, B2, C1, C2, D1, D2), each of them having 12 GHz bandwidth (6-18 GHz) with the frequency of the channels increasing monotonically towards the end of the band. The separation between channels varies from 1 GHz at the beginning of the band to 2 GHz towards the end of the band. The corresponding JPF names and the frequency of each of the channels can be found in Appendix A (tables A1 and A2). This new arrangement allows connecting the high frequency receivers (M7-M12) to a 12 channels filter bank while the low frequency ones (M1-M6) keep using a 24 channel filter bank. With M7 and M8 both possibilities (12 or 24 channels filter bank) are available.

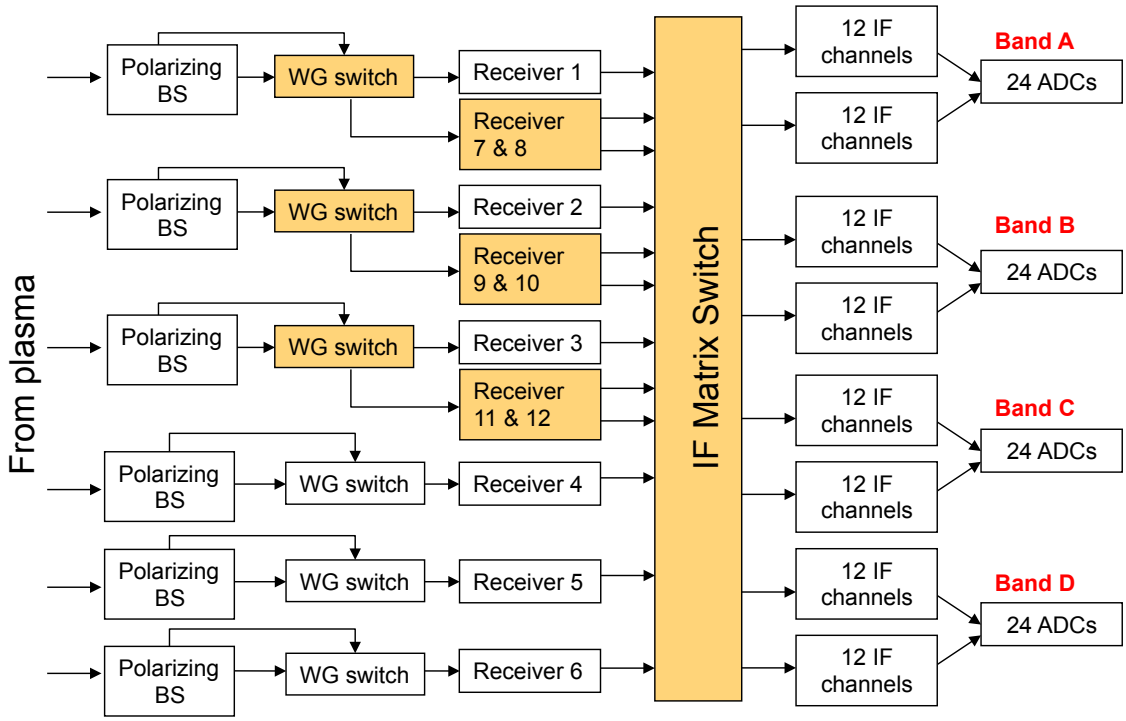

Figure 4. Schematic layout of the new KK3 diagnostic (BS: Beam Splitter, WG:Waveguide). The new hardware added to the radiometer is highlighted.

4.2.1. **Operation and control of the IF waveguide switches** The radiometer uses 6 motorized waveguide switches (manufactured by FLANN, model no.: 28333-xE, with x=2 or 3 depending on the number of channels) connected to the output waveguide after the beam splitters (see figure 4). All the waveguide switches are remotely controlled via GPIB. A combination of 3-ways and 2-ways switches is used to obtained all the required combinations. The 2-ways waveguide switched are connected to a single receiver and, as in the original design, they are used to select the polarization of the radiation to be used for the measurements, either O-mode or X-mode. The 3-channels waveguide

switches, on the other hand, are connected to three receivers (see figure 4). In this case the switches not only control the polarization of the detected radiation but also which of the mixers will be connected to the acquisition chain. It should be noted that way the switches are connected to the output waveguide is different for the 2-ways and the 3-ways switches and therefore they have different settings. The available options are illustrated in figures 5 to 7.

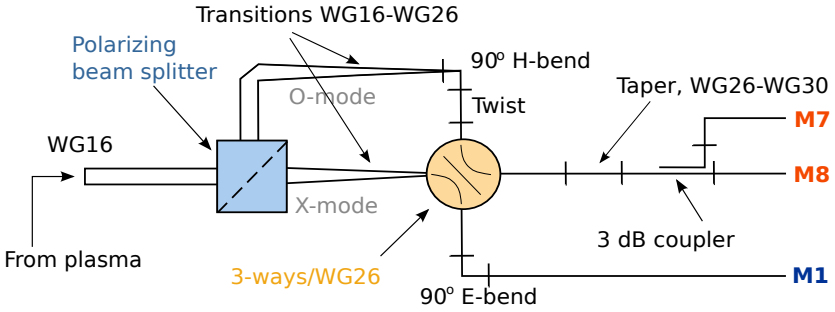

Figure 5. Schematic set-up for the waveguide switch controlling the polarization of receivers M1, M7 and M8 (see table 1). Similar set-up is used for receivers M3, M11 and M12 but the waveguide switch uses band WG28 (90-140 GHz) instead of WG26 (60-90 GHz)

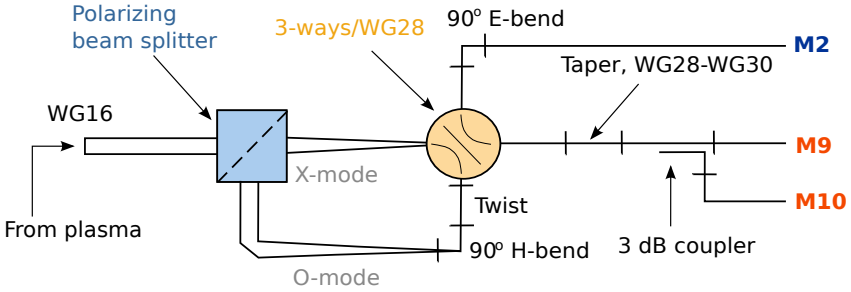

Figure 6. Schematic set-up for the waveguide switch controlling the polarization of receivers M2, M9 and M10 (see table 1).

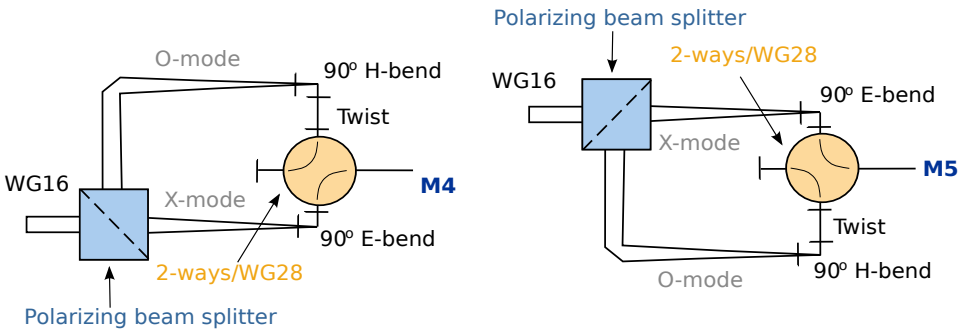

Figure 7. Schematic set-up for the waveguide switch controlling the polarization of receivers M4 (right) and M5 or M6 (left) (see table 1).

4.2.2. **IF switch matrix design.** The selection of which receivers is connected into the acquisition chain is performed by a blocking switch matrix capable to provide automatic routing of signals between the output of the 12 receivers and 8 filter banks (12 channel per filter bank, 96 channels in total), so that at any time a subset of 4, 5 or 6 receivers could be used for the measurements. The switch matrix can be controlled remotely via a GPIB interface. The possible combinations implemented in the IF switch matrix routine are shown in table 2, where:

(a) M1 to M12 are the outputs of the receivers connected to the matrix input channels. For receivers M1 to M8 the power is divided into two by power dividers before entering the switch matrix (denoted by adding 'a' and 'b' to the receiver name in table 2)

(b) A1, A2, B1, B2, C1, C2, D1, D2 represent the matrix output channels, each of them connected to a 12 channels IF filter bank

(c) IS1 to IS8 are the 2-ways IF input switches used in the matrix

(d) OS1 to OS4 are the 4-ways IF output switches used in the matrix

A diagram describing the signal routing architecture is shown in figure 8.

4.3. KK3 control software

The control capabilities of the previous system are retained with the upgrade and the necessary changes have been implemented in the control program in order to include the new hardware. A detailed description of the control software can be found in [CODAS-JDN/H(97)30]. The main features of the control software are:

- The software uses two parameters: the central toroidal field (B_0) and the maximum major radius (R_{max}) to estimate the optimum combination of mixers and their polarization to provide the maximum radial coverage.
- With the addition of the new receivers, the choice of the receivers and the radiation polarization for a specific magnetic field is not unique. Table B1 in Appendix B shows all possible combinations. The selection of which mixer is connected to each of the acquisition bands can be performed in two ways:
  (i) Manual mode: It gives access to all available options within the system.
  (ii) Automatic mode: The software chooses consecutive mixers with the minimum RF frequency being determined by the magnetic field at R_{max}. There are two possible options:
    – Post 2008: this includes the new receivers and it selects the combination that maximize the number of mixers operating in X-mode
    – Pre 2008: it only uses M1 to M6

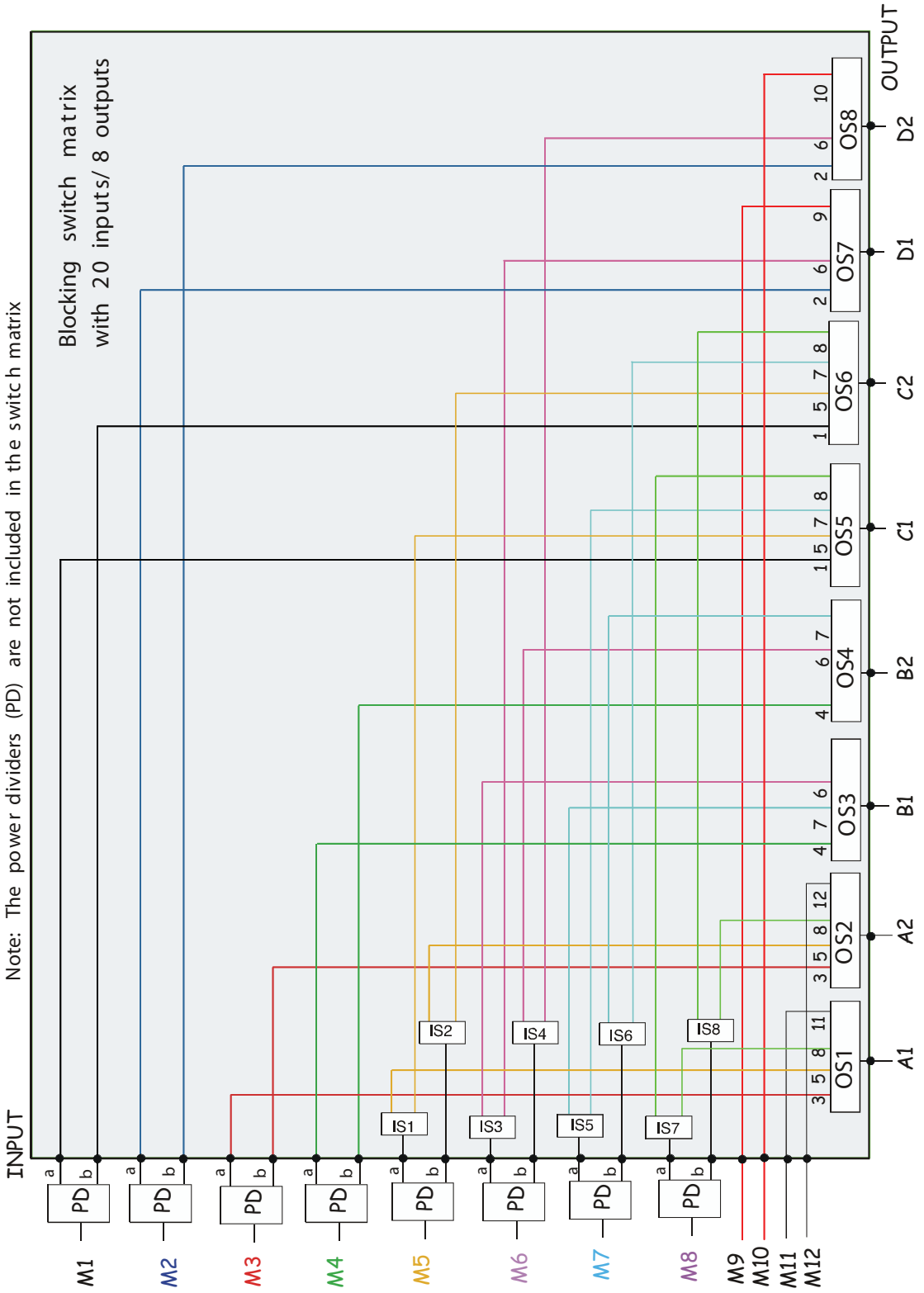

Figure 8. Matrix switch block diagram

	A1	**A2**	**B1**	**B2**	**C1**	**C2**	**D1**	**D2**
M1a					$OS5_1$			
M1b						$OS6_1$		
M2a							$OS7_1$	
M2b								$OS8_1$
M3a	$OS1_1$							
M3b		$OS2_1$						
M4a			$OS3_1$					
M4b				$OS4_1$				
M5a	$OS1_2$ $IS1_1$				$OS5_2$ $IS1_2$			
M5b		$OS2_2$ $IS2_1$				$OS6_2$ $IS2_2$		
M6a			$OS3_3$ $IS3_1$				$OS7_2$ $IS3_2$	
M6b				$OS4_3$ $IS4_1$				$OS8_2$ $IS4_2$
M7a			$OS3_2$ $IS5_2$		$OS5_3$ $IS5_2$			
M7b				$OS4_4$ $IS6_1$		$OS6_3$ $IS6_2$		
M8a	$OS1_3$ $IS7_2$				$OS5_4$ $IS7_1$			
M8b		$OS2_3$ $IS8_2$				$OS6_4$ $IS8_1$		
M9							$OS7_4$	
M10								$OS8_4$
M11	$OS1_4$							
M12		$OS2_4$						

Table 2. Signal routing topology for the switch matrix. The inputs are connected to the 12 receivers (M1 to M12) and the outputs are connected to the 8 filter banks (A1, A2, B1, B2, C1, C2, D1, D2). The subindex in the switch names indicates the IF switch input port

5. Experimental results

The ECE JET radiometer provides detailed information on the plasma electron temperature profile with good spatial (2-5 cm depending on plasma parameters and polarization) [5, 6] and temporal resolution (typically 0.2 ms). The upgraded radiometer began its operation in June 2008. Here we describe how the modifications implemented in the instrument have expanded and improved the range of electron temperature measurements available in JET.

With the use of the new, higher frequency receivers (M7 to M12 in table 1), the usable range of 2X-mode ECE has now been extended up to $B_0 = 4$ T in the pedestal region and up to 3.6 T in the plasma core, covering radii from the outer edge inward to

the location of the third harmonic overlap on the high field side (R_{min} ~2.6 m). The option that uses the maximum number of mixers in X−mode polarization is now the standard option for the instrument during JET operation. But both options (6 mixers or 12 mixers) are available (for B_0 >2.5 T) and can be remotely selected from the Control Room. Figure 9 shows the comparison of the frequency coverage for the original and the upgraded system for two magnetic fields in JET: B_0 = 2.5 T and 3.3 T. Table 3 shows the automatic selection of receivers/polarizations carried out by the radiometer control software.

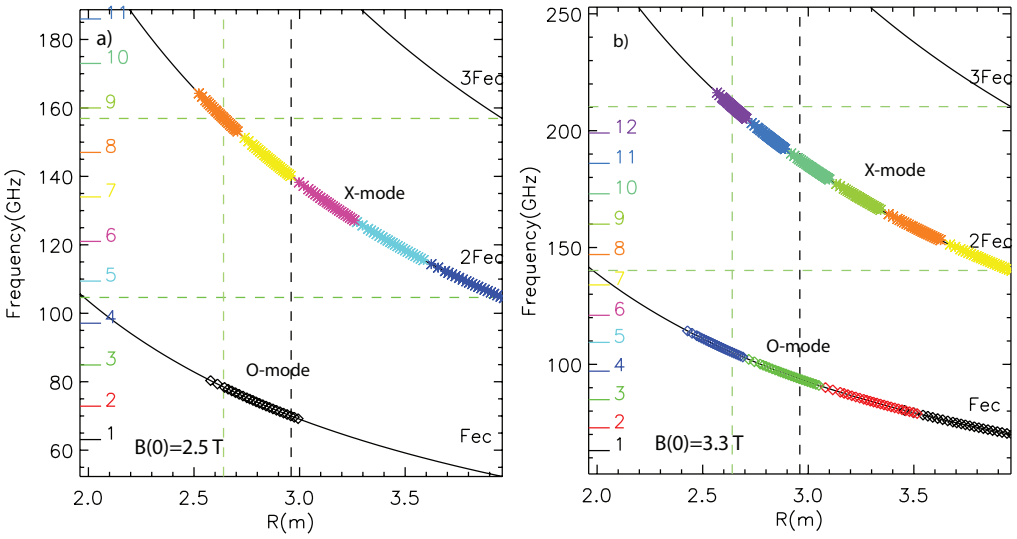

Figure 9. Radial profile of the electron cyclotron frequency and its harmonics for two magnetic fields: (a) B_0 = 2.5 T and (b) B_0 = 3.3 T. The LO frequency together with the radial coverage of the available receivers are shown in different colors. Maximum frequency for the 2X-Mode limited by the overlap with the third harmonic, shown as a vertical green line in the figure.

B_0(T)	**'Pre-2008'** **(6 receivers)**	**'Post-2008'** **(12 receivers)**
2.5	M4X-M5X-M6X-M1O	M4X-M5X-M6X-M7X-M8X
3.3	M1O-M2O-M3O-M4O	M7X-M8X-M9X-M10X-M11X-M12X

Table 3. Available mixer/polarization combination with the upgraded radiometer in JET for two values of the central magnetic field (see figure 9).

5.1. Increased radiometer operational parameter space (access to higher density plasma)

By extending the use of 2X-mode, the range of accessible densities at which reliable T_e measurements from ECE has doubled with respect to the previous system. This increase in the radiometer operational space is illustrated in figure 10, where the electron

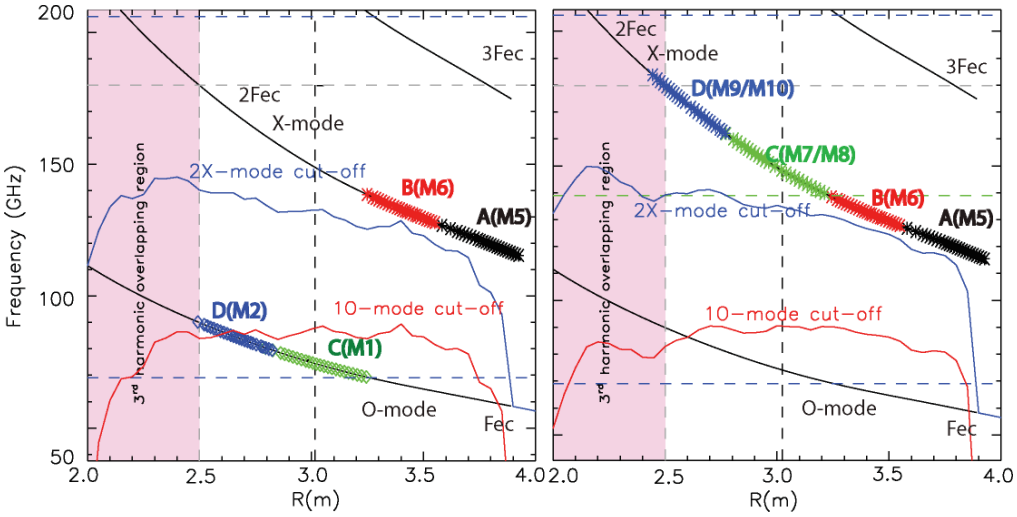

Figure 10. Radial profile of the electron cyclotron frequency, its harmonics and cutoff frequencies for O-mode and X-mode for two pulses with B_0=2.7 T: #73076 at t=18.86 sec (on the right) and #73084 at t=21.63 sec (on the left). The radial coverage of the selected receivers is shown in different colours. A, B, C and D refer to the 4 acquisition bands, with 24 channels per band (O-mode: diamonds, X-mode: crosses).

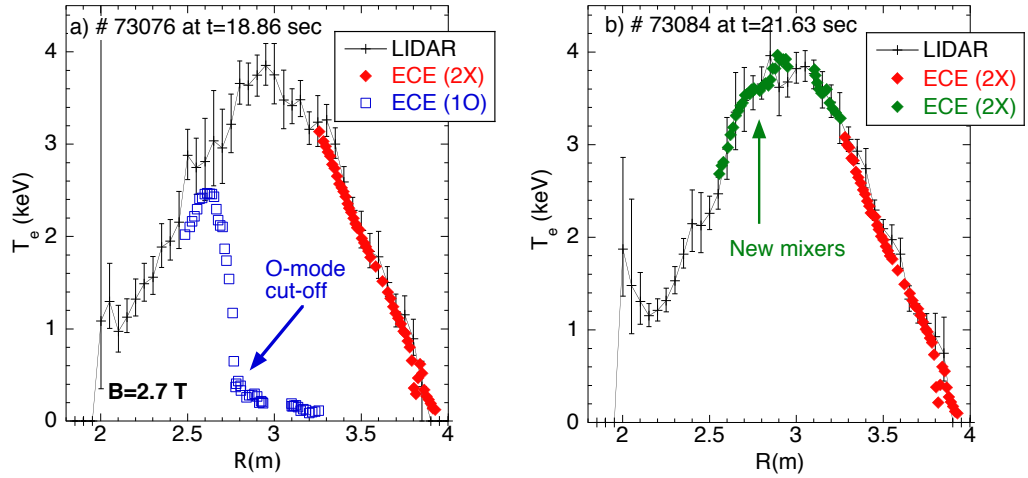

Figure 11. T_e profiles measured by the LIDAR and the ECE radiometer for the pulses shown in figure 10 (O-mode ECE: Open symbols, X-mode ECE: closed symbols).

cyclotron frequencies and its harmonics, together with the cutoff frequencies for O- and X-mode are shown for two JET pulses: #76076 and #76084 with $B_0 = 2.7$ T. These pulses have similar plasma parameters ($P_{NBI} \sim 22$ MW, $n_{e0} \sim 9 \times 10^{19}$ m^{-3}) but the radiometer was configured to use different mixer/polarization combinations. The corresponding T_e profiles measured by the radiometer are shown in figure 11. For pulse #76076 only the low frequency mixers (M1 to M6) were used, to mimic the operation of the radiometer before the upgrade. In this case, 1O-mode emission is used to access the central plasma region, whereas for the second pulse (#76084) the radiometer setup included the new high frequency receivers (M7 to M10), allowing T_e measurements to

be obtained using the 2X-mode radiation. For these plasma conditions, the density is high enough for the 1O-mode emission to be in cutoff but too low to affect the 2X-mode ECE measurements, as it is reflected by the good agreement found between the T_e profile measured by the radiometer and the Thomson Scattering diagnostic.

5.2. Improved access to the edge plasma region at high magnetic fields

Due to the drop of the optical depth towards the plasma edge (strong dependence on n_e and T_e), there is always a limit on how close to the plasma edge ECE can be used for T_e measurements. However, since the optical thickness of the 2X-mode emission is larger than that of the 1O-mode, the region in which reliable edge pedestal T_e measurements can be obtained is larger for the 2X-mode ECE measurements. The benefits of using 2X-mode emission for edge T_e measurements is clearly shown in figure 12, where the T_e profiles measured by the radiometer for two pulses with $B_0 = 3.45$ T and similar plasma conditions (I_p=2.5 MA, P_{ICRH}= 3.5 MW, $n_{e0} = 3 \times 10^{19}$ m^{-3}) are compared. In one case figure 12(a), the radiometer uses the new high frequency downconverters (M7 to M12 in X-mode and M4 in O-mode), while in the other case (figure 12(b)) it uses the mixers available before the upgrade (M3 to M6 in O-mode). The region with 'enhanced' radiation (with $T_{rad} \gg T_e$) that is observed close to the separatrix in figure 12(b) is a well known ECE instrumental effect that appears systematically in the pedestal region (large temperature and density gradients) at the low field side in H-mode plasmas. This effect is well reproduced by the emission code SPECE [7] and can be attributed to relativistically downshifted thermal emission located at smaller radii that is not fully reabsorbed due to the insufficient optical depth at the plasma edge (see [6] for more details).

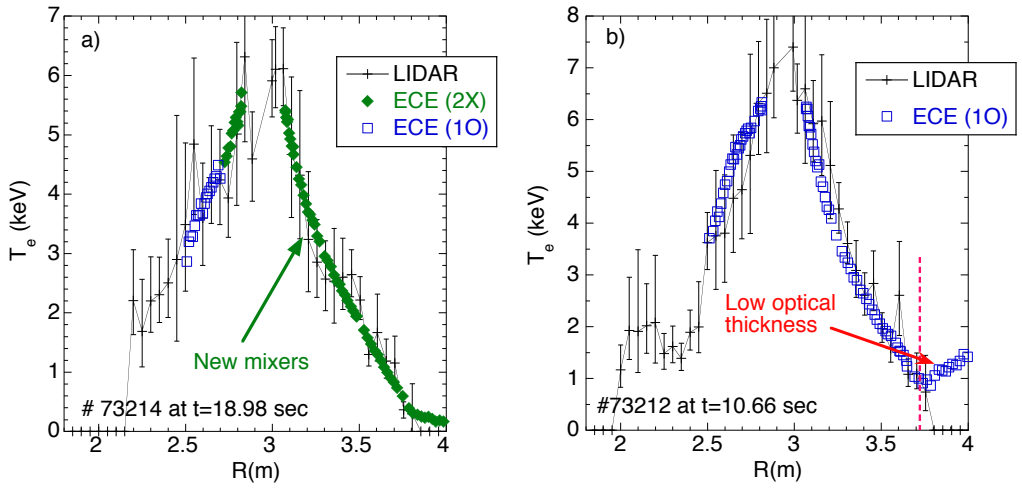

Figure 12. T_e profiles measured by ECE for two pulses with similar plasma conditions (B_0=3.45T, $n_{e0} = 3 \times 10^{19}$ m^{-3}) but using different mixer/polarization combinations in the radiometer: a) M7-M12 in X-mode, M4 in O-mode and b) M1-M4 in O-mode.

5.3. T_e pedestal measurements in high current experiments

The capability of the upgraded radiometer to allow 2X-mode ECE measurements at higher magnetic fields is particularly relevant for high current experiments in JET, where T_e measurements in the pedestal region with high temporal resolution were not possible before the 2008 upgrade. For those experiments the density is not an independent variable, increasing with the plasma current. At 3.2 T the cutoff density for the O-mode in the pedestal region is $\sim 9 \times 10^{19}$ m^{-3}, a value which is often exceeded in high current plasmas. The situation has now changed with the upgraded diagnostic. Figure 13 shows the temporal evolution of the T_e profile during a large Edge Localized Mode (ELM) measured by the radiometer (2X-mode, using receivers M7 to M12) in a pulse with plasma current of 3.8 MA. The better spatial resolution of the 2X-mode emission, together with the high temporal resolution provided by the radiometer, are clearly beneficial for the T_e measurements in the pedestal region, where the demands for radial and temporal resolution in profile diagnostics are extremely high. Further details on the spatial resolution of the ECE measurements can be found in [5, 6]. As a by-product of the upgrade an improved radial coverage (smaller channel separation) is also obtained for a small range of magnetic field (3.1-3.3 T), which is very useful for profiles with steep gradients as the one shown here.

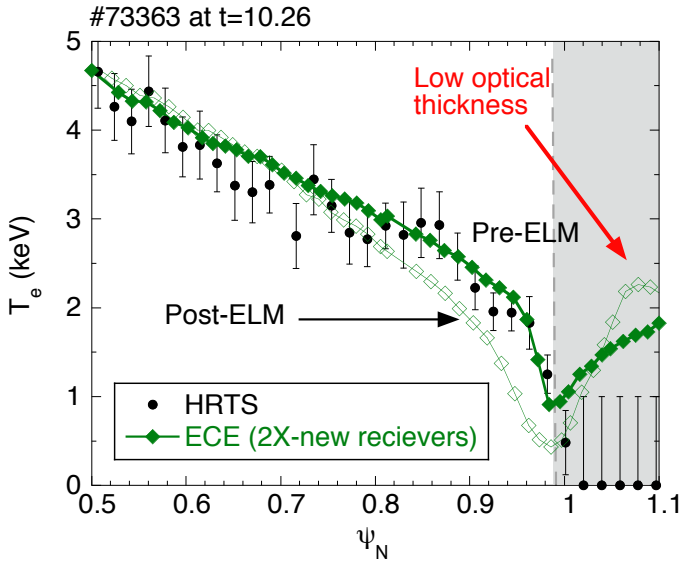

Figure 13. T_e profile evolution during an ELM measured with the upgraded ECE radiometer (M7 to M12 in X-mode) during a high current experiment in JET (B_0=3.2T, I_p=3.8 MA, $n_{e,ped} = 5.5 \times 10^{19}$ m^{-3}). Pre-ELM data: closed symbols ($t = t_{ELM}$) and post-ELM data (maximum T_e drop): open symbols ($t = t_{ELM}$+0.3 ms). The ECE measurements for $\psi_N > 0.99$ can not be interpreted as T_e due to the low optical thickness in that region.

5.4. Good S/N ratio and improved stability

Since the amount of signal distributed between the different receivers has not significantly changed with respect to the original design, the data quality, quantified in terms of S/N ratio, obtained with the new high frequency receivers was very similar to the one obtained with the existing ones.

The radiometer is not absolutely calibrated in stand-alone fashion. Instead it is calibrated by comparison with ECE measurements obtained from the JET Michelson interferometer. This was mainly due to the poor gain stability of the instrument. With the previous system variations in the calibration factors up to +/- 10% were observed during a period of a day. The performance of the receivers are strongly dependent on their physical temperature, this effect being particularly strong for the IF amplifiers. With the installation of the new IF amplifiers, with improved characteristics in terms of noise figure and thermal stability, the situation has considerably improved and calibration characteristic has been observed to remain stable for several JET experimental sessions at a time (for fixed polarization/mixer combinations).

Acknowledgments

The first author wishes to warmly acknowledge the good collaboration between all parties involved in this project (CIEMAT, JOC and CSU). This work has been funded by EFDA under the contracts JW6-OEP-CIEM-14/17 and JW6-NEP-CIEM-11/13.

Appendix A. List of IF channels: frequency and name

The JET radiometer collects data from up to 96 channels, divided into four acquisition bands: A, B, C and D. Each band is subdivided into two sub-bands (12 channels each) with frequencies increasing monotonically from 6 GHz to 18 GHz. Within each band each channels is identified by its frequency and channel name (PPF name).

PPF name Band A	**PPF name Band C**	**Frequency (GHz)**
TE01	TE49	6.125
TE02	TE50	6.946
TE03	TE51	7.768
TE04	TE52	8.589
TE05	TE53	9.411
TE06	TE54	10.232
TE07	TE55	11.054
TE08	TE56	11.875
TE09	TE57	12.75
TE10	TE58	13.75
TE11	TE59	14.75
TE12	TE60	16.25
TE13	TE61	6.55
TE14	TE62	7.35
TE15	TE63	8.17
TE16	TE64	9
TE17	TE65	9.82
TE18	TE66	10.65
TE19	TE67	11.45
TE20	TE68	12.25
TE21	TE69	13.25
TE22	TE70	14.25
TE23	TE71	15.25
TE24	TE72	17.5

Table A1. Central frequencies for filter bank in bands A and C

PPF name Band B	**PPF name Band D**	**Frequency (GHz)**
TE25	TE73	6.325
TE26	TE74	7.15
TE27	TE75	7.975
TE28	TE76	8.89
TE29	TE77	9.6
TE30	TE78	10.45
TE31	TE79	11.175
TE32	TE80	12
TE33	TE81	13.0
TE34	TE82	14.0
TE35	TE83	15.0
TE36	TE84	16.0
TE37	TE85	6.75
TE38	TE86	7.5
TE39	TE87	8.425
TE40	TE88	9.2
TE41	TE89	10.025
TE42	TE90	10.77
TE43	TE91	11.6
TE44	TE92	12.5
TE45	TE93	13.5
TE46	TE94	14.5
TE47	TE95	15.5
TE48	TE96	17.0

Table A2. Central frequencies for filter bank in bands B and D

Appendix B. Available mixers/polarization combinations after the 2008 radiometer upgrade

	1	**2**	**3**	**4**	**5**	**6**	**7**	**8**	**9 10**	**11 12**	**Mixers/Polarization**	B_0
1	C	D	A	B							1X-2X-3X-4X	1.7-19
2		D	A	B	C						2X-3X-4X-5X	2
3			A	B	C	D					3X-4X-5X-6X	2.1-2.3
4	C	D	A	B							3X-4X-1O-2O (LFS/HFS)	
5	C			B	A	D					4X-5X-6X-1O	2.4-2.6
6		D	A	B	C						4X-5X-2O-3O (LFS/HFS)	
7				B	A	D	C				4X-5X-6X-7aX-7bX	
8				B	A	D	C_1	C_2			4X-5X-7aX-8aX	
9	C	D			A	B					5X-6X-1O-2O	2.7-2.9
10			A	B	C	D					5X-6X-3O-4O (LFS/HFS)	
11					C	D	B	A			5X-6X-7aX-7bX-8aX-8bX	
12					A	B	C_1	C_2	D		5X-6X-7aX-8aX-9x-10X	
13	C				A	B			D		5X-6X-1O-9x-10X	
14		D			A	B	C_1	C_2			5X-6X-7aX-8aX-2O	
15	C	D	A			B					6X-1O-2O-3O	3-3.2
16	C			B	A	D					6X-1O-4O-5O (LFS/HFS)	
17						B	C	A	D		6X-7X-8X-9X-10X	
18						B	C_1	C_2	D	A	6X-7X-8X-9X-10X-11X-12X	
19				B	A	D	C1	C2			6X-7X-8X-8bX-4O-5O	
20	C					B			D	A	6X-1O-9x-10X-11X-12X	
21		D				B	C_1	C_2		A	6X-7X-8X-2O-11X-12X	
22			A			B	C_1	C_2	D		6X-7X-8X-9x-10X-3O	
23	C	D				B				A	6X-1O-2O-11X-12X	
24	C	D	A	B							1O-2O-3O-4O	3.3-3.5
25			A				B	C	D		7X-8X-9X-10X-3O	
26							B	C	D	A	7X-8X-9X-10X-11X-12X	
27	C			B					D	A	1O-9X-10X-11X-12X-4O	
28		D		B			C_1	C_2		A	7X-8X-2O-11X-12X-4O	
29			A	B			C_1	C_2	D		7X-8X-9X-10X-3O-4O	
30	C	D		B			C_1	C_2		A	1O-2O-11X-12X-4O	
31	C		A	B					D		1O-9X-10X-3O-4O	
32		D	A	B			C_1	C_2			7X-8X-2O-3O-4O	
33				B			C		D	A	8X-9X-10X-11X-12X-4O	
34		D		B			C		D		8X-2O-11X-12X-4O	
35			A	B			C		D		8X-9X-10X-3O-4O	
36		D	A	B			C			A	8X-2O-3O-4O	
37		D	A	B	C						2O-3O-4O-5O	3.5-3.8
38				B	C				D	A	9X-10X-11X-12X-4O-5O	
39		D		B	C					A	2O-11X-12X-4O-5O	
40			A	B	C				D		9X-10X-3O-4O-5O	
41			A	B	C	D					3O-4O-5O-6O	3.8-4
42				B	C	D				A	11X-12X-4O-5O-6O	

Table B1. All possible mixer/polarization combinations than can be selected by the radiometer control software (in Manual Mode). Combinations available with the existing system (pre 2008) are shown in blue. Specific settings to obtain T_e pedestal measurements from the Low Field Side (LFS) and the High Field Side (HFS) region simultaneously are shown in red.

References

[1] D. V. Bartlett *et al.*, *The JET ECE heterodyne radiometer and investigations of fast phenomena*, in Proc. 8th Joint Workshop on ECE and ECRH, Gut Ising, Germany (1992). JET-C(93)01 (1993).

[2] D. V. Bartlett *et al.*, *Recent Progress in the Measurement and Analysis of ECE on JET*, in Proc. 9th International Workshop on ECE and ECRH, Borrego Sprins, USA (1995). JET-P(95)17 (1995).

[3] E. de la Luna *et al.*, *Electron cyclotron emission radiometer upgrade on the Joint European Torus (JET) tokamak*. Rev. Sci. Instrum. **75**, 3831 (2004).

[4] E. de la Luna, *Physics of ECE Temperature Measurements and Prospects for ITER*, in Proc. International Conference on Burning Plasma Diagnostics (Varenna, 2007). EFDA-JET-CP(07)04/09. AIP Conference **988**, 63 (2008).

[5] V. Tribaldos, *Spatial Resolution of the Electron Cyclotron Emission at JET*. EFDA-JET-PR(01)44 (2001).

[6] L. Barrera *et al.*, *Inboard and outboard electron temperature profile measurements in JET using ECE diagnostics*. Plasma Physics and Controlled Fusion **52**, 085010 (2010).

[7] D. Farina, L. Figini, P. Platania, and C. Sozzi, *SPECE: a code for Electron Cyclotron Emission in tokamaks*, in Proc. International Conference on Burning Plasma Diagnostics (Varenna, 2007). AIP Conference Proceedings **988**, 128 (2008).